Characterization of PLD grown WO_3 thin films for gas sensing

Stefan I. Boyadjiev[1,2]*, Velichka Georgieva[1], Nicolaie Stefan[3], George E. Stan[4], Natalia Mihailescu[3], Anita Visan[3], Ion N. Mihailescu[3], Cristina Besleaga[4], and Imre M. Szilágyi[2,5]

[1]*Institute of Solid State Physics, Bulgarian Academy of Sciences, 72 Tzarigradsko chaussee blvd., 1784 Sofia, Bulgaria*

[2]*MTA-BME Technical Analytical Chemistry Research Group, Szent Gellért tér 4, Budapest, H-1111, Hungary*

[3]*National Institute for Lasers, Plasma and Radiation Physics, 409 Atomistilor Street, Magurele-Ilfov, RO-077125, Romania*

[4]*National Institute of Materials Physics, 405A Atomistilor Street, Magurele-Ilfov, RO-077125, Romania*

[5]*Budapest University of Technology and Economics, Department of Inorganic and Analytical Chemistry, H-1111 Budapest, Szent Gellért tér 4, Hungary*

E-mail: boiajiev@gmail.com

Abstract: Tungsten trioxide (WO_3) thin films were grown by pulsed laser deposition (PLD) with the aim to be applied in gas sensors. The films were studied by atomic force microscopy (AFM), X-ray diffraction (XRD), Fourier transform infrared (FTIR) spectroscopy and profilometry. To study the gas sensing behavior of these WO_3 films, they were deposited on quartz resonators and the quartz crystal microbalance (QCM) method was applied to analyze their gas sensitivity. Synthesis of tetragonal-WO_3 films starting from a target with predominantly monoclinic WO_3 phase was observed. The films deposited at 300 °C presented a surface topology favorable for the sorption properties, consisting of a film matrix with protruding craters/cavities. QCM prototype sensors with such films were tested for NO_2 sensing. The PLD grown WO_3 thin films show good sensitivity and fast reaction at

room temperature, even in as-deposited state. With the presented technology, the manufacturing of QCM gas sensors is simple, fast and cost-effective, and it is also suitable for energy-effective portable equipment for on-line monitoring of environmental changes.

Keywords: *gas sensor, quartz crystal microbalance, pulsed laser deposition, thin film, WO_3*

1. Introduction

Tungsten trioxide (WO_3) is one of the most widely studied semiconductor oxides, due to its remarkable physical, optical and optoelectronic properties [1–2]. WO_3 grown as thin film can be used for various applications, such as electrochromic devices (in displays, smart windows and optical switching coatings) [1–3], sensing numerous toxic and inflammable gases [4–7], photocatalysis [8–9], solar energy conversion [2], water splitting [10], and many others.

The quartz crystal microbalance (QCM) is a widely-used technique for detecting the mass of thin films deposited on the crystal surface in the sub-nanogram range, but it could be also applied for monitoring the adsorption of very small amounts of various toxic gases. When the QCM method is used for gas sensing, the surface properties of the sensing material are of higher importance, compared with its bulk. Very thin films are also applicable for gas sensors [11–12], while their morphology is of high importance. Also, compared with other methods, the advantages of QCM for sensing gases are the high sensitivity, simple technological implementation and easy real-time monitoring, capability of operating at room temperature, relative independence from electromagnetic fields and rapid temperature changes, fast response even at low concentrations, durability, portability, low energy consumption and cost [13–14].

Although WO_3 shows good sensitivity to many gases [4–7], it is possible to further improve its gas sensing properties by fostering its nanostructured morphology to increase the specific surface area. Therefore, already various techniques have been adopted to grow thin films from oxide materials with higher specific surface area.

Pulsed laser deposition (PLD), also called deposition by laser ablation, is a physical vapor deposition (PVD) process based on the vaporization of condensed matter by means of photons [15–17]. A highly intense short-pulsed (usually of nano- or pico-seconds)

high-power laser beam is focused under vacuum or a working gas atmosphere on a target of the deposited material. If the laser fluence exceeds a specific threshold, the ablated material is directed forward, in form of a plume, towards the deposition substrate, where film is formed by re-condensation [15–16].

As the species arriving on the substrate are highly energetic, the synthesized films elicit high adherence. Moreover, the plasma plume plays a notable piston-like role, pushing and carrying the removed matter from the ablated target to the substrate [16].

PLD is a versatile PVD method which presents a distinct set of advantages, which currently increases its appeal in the sensors field. The main ones are: i) congruent target-to-substrate transfer of substances with intricate stoichiometries; ii) control over the growing films morphology by adapting the deposition variables (possibility for growth of rough or nanostructured surfaces); and iii) plasma direct action upon surface can result in a rather large hardness, along with a high adherence of the growing film to the substrate.

i) The first feature is particularly important in the case of WO_3, which could be chemically modified during transfer. However, as shown in our previous studies [18], ns excimer laser pulses can promote the growth of stoichiometric WO_3 film on substrate after laser transfer.

ii) The deposition of substance in form of nanoparticles covering the surface of film is a characteristic of PLD, which can facilitate the natural growth of nanostructured surfaces with an increased active area beneficial for gas sensing [19–21].

iii) The films obtained by PLD after the plasma transfer are usually very adherent to substrate and also have a rather large hardness, which is of key importance for the long term use as gas sensors in specialized devices [17, 22–23].

Therefore, in the present study PLD was chosen as method allowing the growth of highly pure and adherent thin films with larger surface area, which is more beneficial morphology for gas sensing, compared with other PVD methods.

The usual PLD drawbacks are the rather non-uniform thickness distribution, the possible presence of bigger size (submicronic or even micronic) droplets and the rather limited deposition area of usually only few square centimeters [15–16]. But when preparing QCM gas sensors none of these limitations are significant for the fabricated device, since of high importance are only the surface properties of the films, and the active sensing area of the

QCM sensor is rather small.

Reactive PLD is a strategy to enhance the reactivity between the background gas and the ablated species in order to reconstitute on the substrate the stoichiometry of the likely lost elements in the deposited films. For example, due to its expansion velocity, the lighter oxygen species develop a larger angular distribution in the plume than the heavier elements, such as tungsten, and additional sources to compensate the expected oxygen loss can be necessary [15–17].

In this study, we prepared QCM gas sensors with PLD grown WO_3 thin films, which were characterized by atomic force microscopy (AFM), X-ray diffraction (XRD), Fourier transform infrared (FTIR) spectroscopy and profilometry. The gas sensing was investigated by detecting various concentrations of NO_2 in dry air at room temperature.

2. Experimental methods

2.1 Preparation of the gas sensors

Previously, prototype QCM gas sensors with several transition metal oxide films (e.g. TiO_2, MoO_3, ZnO) were already fabricated by our team and tested for sensitivity to NO_2 in a specially designed experimental set-up [24]. These films were mostly prepared by reactive magnetron sputtering [25–26] and atomic layer deposition (ALD) [11–12]. In the present study, we focused on the sensing behavior of WO_3 thin films grown by PLD. Such films were deposited either on quartz resonators (AT-cut 16 MHz QCM with 4 mm gold electrodes on both sides), which were used for preparing the QCM gas sensors [11–12], or on Si substrates, which were used for further characterization of the films. Prior to deposition all substrates were cleaned in an ultrasonic bath with acetone and ethanol for 10 minutes, rinsed in deionized water and finally purged with synthetic air. All depositions were carried out in a standard reactive PLD (RPLD) setup [16] consisting of a stainless-steel vacuum reaction chamber equipped with a gas flow, heating and vacuum pump systems, MgF_2 optics and windows. Before deposition, the reactor chamber was evacuated down to a residual pressure of $\sim 5 \times 10^{-5}$ Pa in order to avoid contamination. Then, a flux of pure O_2 (99.999%) was introduced to attain an oxygen pressure of 16 Pa. A commercial monoclinic WO_3 powder (Fluka, purity 99.99%), compacted at 2 MPa and sintered (1100 ^{o}C for 6 h), was used as target to be ablated by a KrF (248 nm, 25 ns) pulsed laser source at a fluence of 1.2 J/cm^2 and

repetition rate of 40 Hz. The samples were deposited on heated substrates (at 150 or 300 ^{o}C) with a definite number of laser pulses (N), and oxygen pressure in the reactor chamber. The target was rotated at a 0.5 Hz frequency, to avoid its piercing and to assure a smooth ablation procedure. For all experiments a target-to-substrate distance of 40-mm was used. The deposition parameters are summarized in Table 1.

2.2 Characterization techniques

a) The surface morphology of films was analyzed by Atomic Force Microscopy (AFM) in non-contact mode using an NT-MDT NTEGRA Probe NanoLaboratory system (NT-MDT NSG01 cantilever with tip radius of 10 nm).

b) Fourier transform infrared (FTIR) spectrometry studies were performed in transmission mode with a Shimadzu 8400S instrument. The investigated range was chosen between 500–4000 cm^{-1}, with a resolution of 4 cm^{-1}.

c) The structure of the WO_3 films samples was investigated by Grazing Incidence X-Ray Diffraction (GIXRD) using a Bruker D8 Advance diffractometer, in parallel beam setting, with Cu Kα (λ = 1.5418 Å) incident radiation. The incidence angle was set to 2°, and the scattered intensity was scanned within the range (20–60)° (2θ), with a step size of 0.04°, and 6 s per step.

d) The initial parameters of the QCM sensors and their quality were evaluated by measuring the main equivalent dynamic parameters: equivalent dynamic resistance R_q and static capacitance C_0 using a selective level meter. The other parameters, such as the quality factor (Q), were calculated [27]. The QCM gas sensors with PLD grown WO_3 films were installed on a special holder inside the test chamber. The chamber was first evacuated, and then the test gas, with a certain concentration, was released in a continuous flow. The velocities of both the carrier (high purity synthetic air) and test (NO_2) gases were measured and controlled by mass flow controllers, their ratio being defined by the desired concentration. A frequency counter (Hameg 8123) connected to the QCM, as well as to the computer for data recording, registered the QCM frequency. Thus, the frequency change as a function of time was recorded. The gas sensing measurements were based on the correlation between the frequency shift and the additional sorbed mass loading of the resonator. The correlation between the frequency shift (ΔF) and the sorbed mass (Δm) for AT-cut quartz is given by

Sauerbrey equation [28]. This way the sorbed mass can be calculated and the gas sensing can be quantitatively determined. The initial frequency value was considered the one measured in the carrier gas flow, under saturation conditions. The temperature of the QCM was measured by a Pt thermal sensor positioned near the QCM and was maintained constant during the measurements, thus avoiding inaccuracies caused by temperature changes. In order to eliminate selectivity error from sorbed water vapours, first the films were saturated to H_2O (equilibrium in the measured frequency was achieved), and then these values were taken as initial for the NO_2 measurements.

3. Results and Discussion

Our previous studies revealed that the roughness of the resonator electrodes influences the gas sensing properties of the WO_3 thin films [29]. It was concluded that that the optimal conditions can be defined by a compromise between a surface with higher roughness, which has better sorption but slower desorption and decreased quality of the QCM, and smoother one, possessing a decreased sensing ability. Another approach to improve the sorption properties is to design a surface morphology of the sensing film with higher roughness, which is beneficial for the sorption but does not reduce the QCM quality (still, here the desorption speed is also influenced, so optimization is also needed). The PLD method generally offers possibilities for deposition of thin films with higher specific surface area, compared with the previously studied WO_3 films deposited by sputtering. Two different deposition temperatures were used for synthetizing films with different degrees of crystallinity and surface roughness.

The PLD method was found to be suitable for deposition of WO_3 films on QCM for sensor applications. The films were uniform and with good quality and adhesion to the QCM electrodes. The thickness of the films of ~600 nm for the 301 sample and ~1500 nm for the 151 sample was rather high, which is not specifically needed for the sensing properties of the films when using the QCM method (in our previous studies it was found out that much thinner films also have rather good sensing properties when using the QCM method [11–12]). But since the deposition rates while using PLD are rather high compared to many other methods, growing a bit thicker films, which could be better for long term usage, can be easily and cost-effectively facilitated.

Since the surface morphology and roughness is of high importance for the sorption of the gas molecules, the films were first analyzed by AFM. The AFM images, collected at different magnifications (Fig. 1), indicated in the case of WO_3 films deposited at the lower temperature (i.e. 150 °C) a typical PLD morphology composed of closely-packed quasi-equiaxial spherical grains (Fig. 1-a,b). The majority of grains in the case of this type of sample had diameters in the range ~112 – 120 nm, with only scarce cases of extremes, with sizes of ~90 and ~200 nm. Instead, the sample deposited at the higher temperature (i.e. 300 °C) presented a radically different surface topology: a very smooth film matrix with fairly well-distributed protruding craters/dents (Fig. 1-c,d). The topographies presented in Fig. 1 were characteristic for the entire films surface, pointing to a good morphological uniformity. The root mean square roughness (R_{RMS}) of the WO_3 films deposited at 150 °C and 300 °C, determined on the basis of the 10x10 μm^2 AFM images, were of ~17 nm and ~4 nm, respectively.

It is not clear yet why these dents have formed at the films deposited at 300 °C. It might be due to a desorption process of species arriving at the substrate surface, not finding an energy favorable spot, in this case of a higher temperature and fast film structuring process. Or some substrate topological defects could act as energy barriers for some species, and as they do not find the energy favorable site, they desorb. Thus, in such spots, the deposition rate is lower, and this does not allow for the films to fill out the substrate voids. In any case, such morphology is favorable for the sorption properties of the film, though it can be assumed that the desorption times could be also increased.

The FTIR spectra of the source powder and sintered PLD target are presented comparatively in Fig. 2a. All absorption bands characteristic to a monoclinic WO_3-type phase were identified: asymmetric stretching (ν_{as}) motions band within the equatorial plane (~646 cm^{-1}), $\nu(W–O_{intra}–W)$ stretching vibrations of the bridging oxygen (~788 cm^{-1}), and $\nu(W–O_{inter}–W)$ stretching vibrations of the bridging oxygens (~866 cm^{-1}) [30–33]. The shallow peaks at ~1012 and ~1040 cm^{-1} are assigned to the stretching of the W=O bonds at the surface of the grains [34–35]. The absorbance bands of the PLD target are both more conspicuous and slightly shifted to higher wave numbers with respect to the raw starting powder, which suggests the increased short-range order of this material. The IR spectra of PLD films (Fig. 2b) displayed a slightly different allure, with the W-O and W=O vibrational stretching bands

maxima somewhat shifted and less defined with respect to ones elicited by the bulk WO_3 materials (Fig. 2a).

The XRD analyses have been carried out in symmetric (θ-θ) geometry on the source powder material and the PLD sintered target (Fig. 3a). The sintering treatment induced an increased crystallization of the WO_3 material, as indicated by the sharper and more defined diffraction peaks. In both powder and target cases, the monoclinic WO_3 phase is the prominent one (ICDD: 01-083-0950), with the triclinic-WO_3 (ICDD: 01-083-0947) present only as a supplemental minor phase. If in the case of the powder, the presence of triclinic-WO_3 is only hinted by some fainted shoulders, in the case of the target, the sintering treatment induces the crystallinity increase of this minor phase, making it easier and safer to be ascertained. (Fig. 3a – inset).

The GIXRD analyses, performed on the PLD films (Fig. 3b), indicated the amorphous status of the WO_3 film deposited at 150°C, at the sensitivity limit of the apparatus. The film deposited at 300 °C consisted of tetragonal WO_3 crystalline phase (ICDD: 01-089-8052). The high intensity of the 002 peak with respect to the reference ICDD file points toward a *c*-axis preferential oriented growth of the crystallites. This is supported also by the modified relative intensities (compared to the ICDD file) of the recorded peaks, as a function of the tilt angle: the absence of reflections of planes perpendicular to c-axis (e.g., 110, 200), and the presence of peaks appertaining to planes tilted with various angles with respect to the surface (e.g., 102, 112, 202, 104, etc). The crystalline coherence length ("crystallite size") was estimated from the full-width at half maximum of the 002 diffraction line using the Scherrer equation. The line width was corrected for instrumental broadening using a corundum standard reference (NIST SRM 1976). A crystalline coherence length of ~51 nm has been calculated. The zoomed region (the intensity scales of the graphical representations were chosen so that to emphasize the low intensity humps), presented in Fig. 3b-inset, indicated that the film deposited at 300 °C, has as well an amorphous minor component.

The crystal structure of WO_3 is temperature dependent: α-WO_3 – tetragonal (~740 – 900 °C), β-WO_3 – orthorhombic (~330 – 740 °C), γ-WO_3 – monoclinic (~17 – 330 °C), δ-WO_3 – triclinic (–43 – 17 °C), and ε-WO_3 – monoclinic (< –43 °C) [36–37]. However, in non-equilibrium thermodynamic conditions, such as the ones typically met in the case of physical vapor deposition methods, obtaining various WO_3 phases outside the

above-mentioned temperature ranges, seems reasonable. The synthesis by PLD of tetragonal-WO_3 films starting from a target with different crystal structure is not unprecedented. Mitsugi et al. [38] has obtained tetragonal-WO_3 films from a triclinic-WO_3 target by PLD in (fairly) comparable deposition conditions.

For a well-working QCM sensor of main importance are: i) the fast and stable response (stable decrease in the frequency when the tested gas is introduced in the chamber); ii) reaching saturation (equilibrium between the sorbed and desorbed molecules of the detected gas at certain concentration) in a reasonable time; and iii) the sorption to be a physical process during which the sensor can be easily recovered (and the initial values for the frequency are reached after the tested gas is removed from the chamber). All these were observed for the presently studied PLD grown WO_3 films. Also, our prototype QCM sensors with PLD deposited WO_3 thin films showed good sensitivity to NO_2. In Fig. 4 and Fig. 5 are presented the frequency-time characteristics (FTCs) of such a QCM sensor measured at 500 and 1000 ppm NO_2 concentrations. They were both typical for a well-working sensor.

At concentration of 500 ppm (Fig. 4) the frequency change until reaching saturation was $\Delta f \approx 50$ Hz. The recovery was complete and the initial values of the resonator were achieved after removing the NO_2 gas from the chamber. The sorption was considered to be a fully physical process, shown by the full recovery of the sensor in a comparably short time.

At higher concentrations the kinetics of the sorption and desorption processes was faster and better expressed (Fig. 5). At a concentration of 1000 ppm, the change of frequency until reaching saturation was $\Delta f \approx 80$ Hz. With increasing NO_2 concentration, the sorption was faster, while the time for reaching dynamic equilibrium was a bit longer, corresponding to the higher adsorbed mass on the film surface. The sorption was still physical and the resonator could be fully recovered, while the recovery times remained almost the same. This shows that the dents present on the surface do not have a negative influence on the desorption process, while most probably being beneficial for the sorption properties.

At both concentrations, the sorption process could be divided in two stages: faster at the beginning and then slower until reaching saturation. The length of the stages was proportional to the sorbed mass and was similar at the both concentration – around 2/3 of the saturation time for the faster stage, and around 1/3 for the slower one.

Since the studied QCM sensors operate at room temperature, they generally do not have

problems with long term cycling as many conductometric sensors, which are working only at high operational temperatures. Similar QCM gas sensors were tested from our team after many years (some after even 7–8 years) and showed similar parameters, proving their ability to detect for many cycles and long terms [25–26].

From our previous studies [11–12, 24–26, 29] and the results from the present one, could be noted that the main advantages of the PLD method for preparing QCM gas sensors in comparison with the others that our team used before are: i) the fast deposition times, which together with the easier and less costly preparation of the PLD target make the method more cost-effective, compared with both the reactive sputtering and ALD; ii) easily prepared nanostructured surface, which was hardly (for longer deposition times and in a smaller degree) achieved by reactive sputtering, something that is of high importance for the sensing properties of the as-grown films.

4. Conclusions

Synthesis by PLD of tetragonal-WO_3 films starting from a target with predominantly monoclinic WO_3 phase was observed. The PLD method was found to be suitable for fast and cost-effective deposition of WO_3 thin films for QCM gas sensors. The films deposited at 300 °C presented a surface topology favorable for the sorption properties, consisting a film matrix with fairly well-distributed protruding craters/cavities. At the same time, it was found that it does not have negative influence on the desorption process. These PLD grown WO_3 thin films showed good sensitivity to NO_2 at room temperature and capability to very well register various concentrations. The sorption was fully reversible and the sensors could be recovered in considerably short time.

Acknowledgments

S.I.B. acknowledges the Postdoctoral Fellowship programme of the Hungarian Academy of Sciences (2013–2015) and the INERA REGPOT Project of Institute of Solid State Physics, Bulgarian Academy of Sciences. N.S., N.M., A.V., F.M.M and I.N.M. acknowledge the Core Program LAPLACE–IV 2016–2017. G.E.S. and C.B. thank the NIMP Core Programme PN 16 48–3/2016. I.M.S. thanks a János Bolyai Research Fellowship of the Hungarian Academy of Sciences and an OTKA–PD–109129 grant.

References

[1] C.G. Granqvist, Handbook of Inorganic Electrochromic Materials, Elsevier, Amsterdam, 1995.

[2] K.A. Gesheva, Thin film optical coatings for effective solar energy utilization, Nova Science, New York, 2007.

[3] P.M.S. Monk, R.J. Mortimer, D.R. Rosseinsky, Electrochromism and Electrochromic Devices, Cambridge university press, Cambridge, 2007.

[4] C. Balázsi, L. Wang, E.O. Zayim, I.M. Szilágyi, K. Sedlacková, J. Pfeifer, A.L. Tóth, P.-I. Gouma, J. Eur. Ceram. Soc. 28 (2008) 913.

[5] M. Blo, M.C. Carotta, S. Galliera, S. Gherardi, A. Giberti, V. Guidi, C. Malagù, G. Martinelli, M. Sacerdoti, B. Vendemiati, A. Zanni, Sens. Actuator B-Chem. 103 (2004) 213.

[6] L. Guatwei, T. Xian-ju, C. Choongyew, A. Gaiktin, A.B.M. Zailani, J. Mater. Sci. Eng. 5 (2011) 27.

[7] I.M. Szilágyi, S. Saukko, J. Mizseic, A.L. Tóth, J. Madarász, G. Pokol, Solid State Sci. 12 (2010) 1857.

[8] Y. Wicaksana, S. Liu, J. Scott, R. Amal, Molecules 19 (2014) 17747.

[9] I.M. Szilágyi, B. Forizs, O. Rosseler, A. Szegedi, P. Nemeth, P. Kiraly, G. Tarkanyi, B. Vajna, K. Varga-Josepovits, K. Laszlo, A.L. Tóth, P. Baranyai, M. Leskelä, J. Catal. 294 (2012) 119D.

[10] B. Marsen, E.L. Miller, D. Paluselli, R.E. Rocheleau, Int. J. Hydrogen Energy 32 (2007) 3110.

[11] S. Boyadjiev, V. Georgieva, L. Vergov, Z. Baji, F. Gáber, I.M. Szilágyi, J. Phys.: Conf. Ser. 559 (2014) 012013.

[12] S.I. Boyadjiev, V. Georgieva, R. Yordanov, Z. Raicheva, I.M. Szilágyi, Appl. Surf. Sci. 387 (2016) 1230–1235.

[13] A. Cunningham, Introduction to Bioanalytical Sensors, Wiley, New York, 1998.

[14] A. Mirmohseni, K. Rostamizadeh, Sensors 6 (2006) 324–334.

[15] C.W. Schneider and T. Lippert, “Laser ablation and thin film deposition”, Chapter 5 in: P. Schaaf (Ed.) “Laser Processing of materials Fundamentals, applications and

developments", Springer series in Materials science 139, Springer, Berlin, 2010, pp. 89–112.

[16] I.N. Mihailescu, E. Gyorgy, "Pulsed Laser Deposition: An Overview", in: "International Trends in Optics and Photonics", T. Asakura (Ed.), Springer, Heidelberg, 1999.

[17] R. Eason, Pulsed Laser Deposition of Thin Films – Applications-Led Growth of Functional Materials, Wiley-Interscience, New York, 2007.

[18] E. György, G. Socol, I.N. Mihailescu, C. Ducu, S. Ciuca, J. Appl. Phys. 97 (2005) 093527.

[19] G. Socol, E. Axente, C. Ristoscu, F. Sima, A. Popescu, N. Stefan, L. Escoubas, J. Ferreira, S. Bakalova, A. Szekeres, I.N. Mihailescu, J. Appl. Phys. 102 (2007) 083103.

[20] A. Klini, V. Zorba, E. Gyorgy, C. Ristoscu, V.S. Teodorescu, I.N. Mihailescu, C. Fotakis, Laser Phys. 13 (2003) 1325–1329.

[21] C. Ghica, C. Ristoscu, G. Socol, D. Brodoceanu, L.C. Nistor, I.N. Mihailescu, A. Klini, C. Fotakis, Appl. Surf. Sci. 252 (2006) 4672–4677.

[22] E. Gyorgy and I. N. Mihailescu, "Enzyme-Based Biosensors for Trace Detection", chapter 9 in "Life Cycle Analysis of Nanoparticles: Risk, Assessment, and Sustainability", A. Vaseashta (Ed.), DEStech Publications, 2015, pp. 231–248.

[23] C. Ristoscu, I.N. Mihailescu, D. Caiteanu, C.N. Mihailescu, T. Mazingue, L. Escoubas, A. Perrone, H. Du, "Nanostructured thin optical sensors for detection of gas traces", chapter 2 in "Functionalized Nanoscale Materials, Devices, & Systems", A. Vaseashta, and I.N. Mihailescu (Eds.), Springer Science + Business Media B.V., 2008, pp. 27–50.

[24] V. Georgieva, P. Stefanov, L. Spassov, Z. Raicheva, M. Atanassov, T. Tincheva, E. Manolov, L. Vergov, J. Optoelectr. Adv. Mater. 11 (2009) 1363–1366.

[25] R. Yordanov, S. Boyadjiev, V. Georgieva, Digest J. Nanomat. Biostruct. 9 (2014) 467–474.

[26] R. Yordanov, S. Boyadjiev, V. Georgieva, L. Vergov, J. Phys.: Conf. Ser. 514 (2014) 012040.

[27] S. Manolov, H. Tihchev, Generators, Tehnika, Sofia, 1982.

[28] G.Z. Sauerbrey, Physik 155 (1959) 206–212.

[29] V. Georgieva, Z. Raicheva, A. Grechnikov, V. Gadjanova, M. Atanassov, J. Lazarov, E.

Manolov, J. Phys.: Conf. Ser. 253 (2010) 012046.
[30] L.M. Bertus, C. Faure, A. Danine, C. Labrugere, G. Campet, A. Rougier, A. Duta, Mater. Chem. Phys. 140 (2013) 49–59.
[31] N. Sharma, M. Deepa, P. Varshney, S.A. Agnihotry, Thin Solid Films 401 (2001) 45–51.
[32] J. Díaz-Reyes, V. Dorantes-García, A. Pérez-Benítez, J.A. Balderas-López, Superficies y Vacío 21 (2008) 12–17.
[33] S.M. Kanan, Z. Lu, J.K. Cox, G. Bernhardt, C.P. Tripp, Langmuir 18 (2002) 1707–1712.
[34] H.I.S. Nogueira, A.M.V. Cavaleiro, J. Rocha, T. Trindade, J.D. Pedrosa de Jesus, Mater. Res. Bull. 39 (2004) 683–693.
[35] U. Opara Krasovec, A. Surca Vuk, B. Orel, Electrochim. Acta 46 (2001) 1921–1929.
[36] H. Kalhori, S.B. Porter, A.S. Esmaeily, M. Coey, M. Ranjbar, H. Salamat, Appl. Surf. Sci. 390 (2016) 43–49.
[37] M.C. Rao, Journal of Non-Oxide Glasses 5 (2013) 1.
[38] F. Mitsugi, E. Hiraiwa, T. Ikegami, K. Ebihara, R.K. Thareja, Jpn. J. Appl. Phys. 41 (2002) 5372–5375.

Table Caption

Table I. Experimental conditions for PLD deposited WO_3 thin films.

Figure Captions

Fig. 1. Characteristic AFM images, collected at different scales (10×10 μm^2 (a,c) and 2×2 μm^2 (b,d)), for the 151 (a,b) and 301 (c,d) WO_3 thin films fabricated by PLD on Si <100> mirror polished substrates.

Fig. 2. Comparative FTIR spectra of (a) WO_3 source powder and sintered PLD target, and (b) WO_3 films deposited by PLD.

Fig. 3. Comparative GIXRD patterns of the (a) source powder and PLD sintered target, and (b) WO_3 films fabricated by PLD at 150 °C and 300 °C. Insets: zoomed selected regions of the GIXRD diagrams.

Fig. 4. FTC of PLD grown at 300 °C WO_3 thin film towards 500 ppm NO_2.

Fig. 5. FTC of PLD grown at 300 °C WO_3 thin film towards 1000 ppm NO_2.

Table I. Experimental conditions for PLD deposited WO_3 thin films.

Sample code	D_{T-S} (mm)	Fluence (J/cm^2)	Repetation rate, f (Hz)	O_2 pressure (Pa)	T (°C)	No. of pulses ($K=10^3$)	Deposition time (sec)
WO_3-151	40	1.2	40	16	150	22 K	550
WO_3-301		1.2			300	8 K	200

Figures:

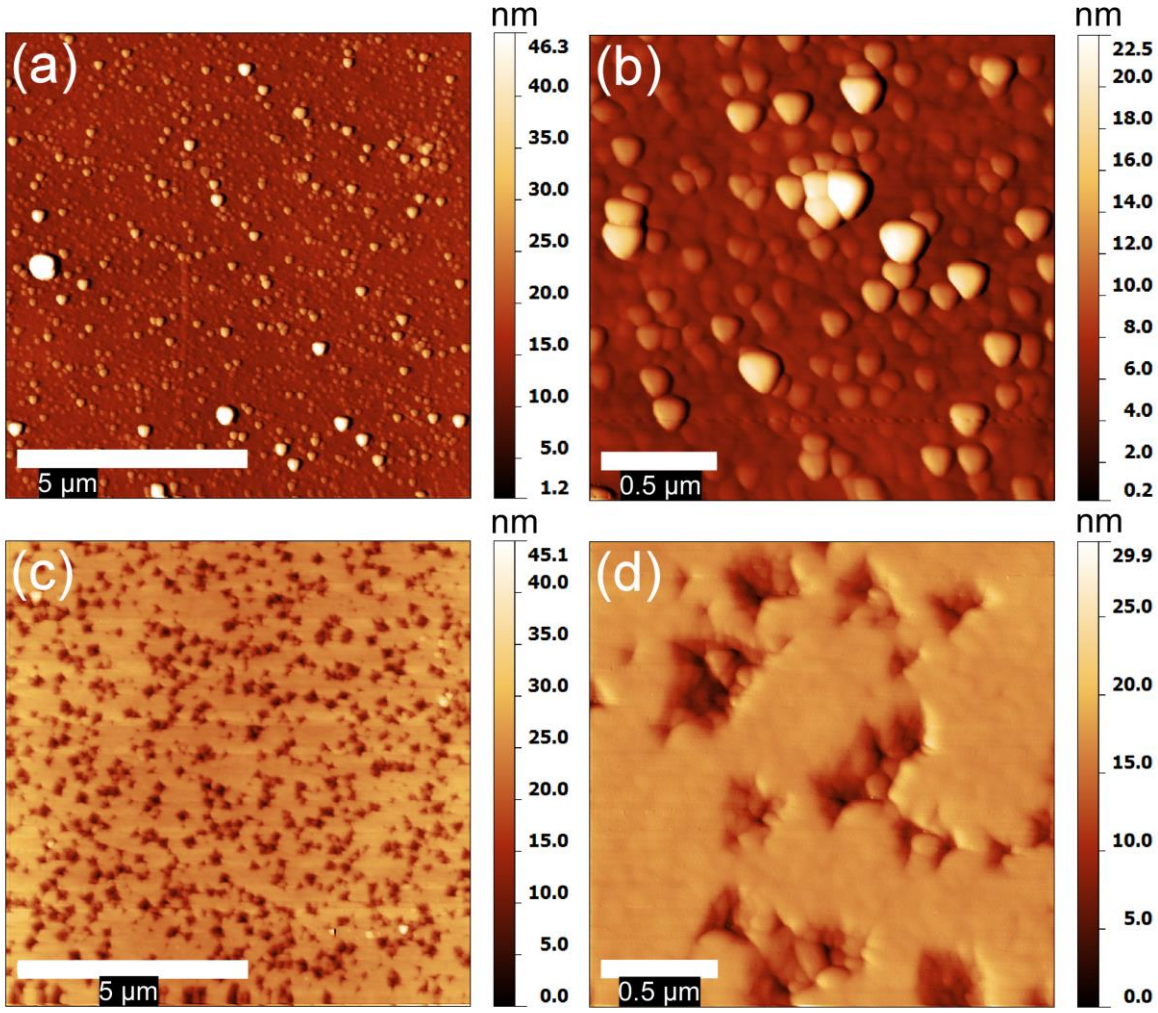

Fig. 1.

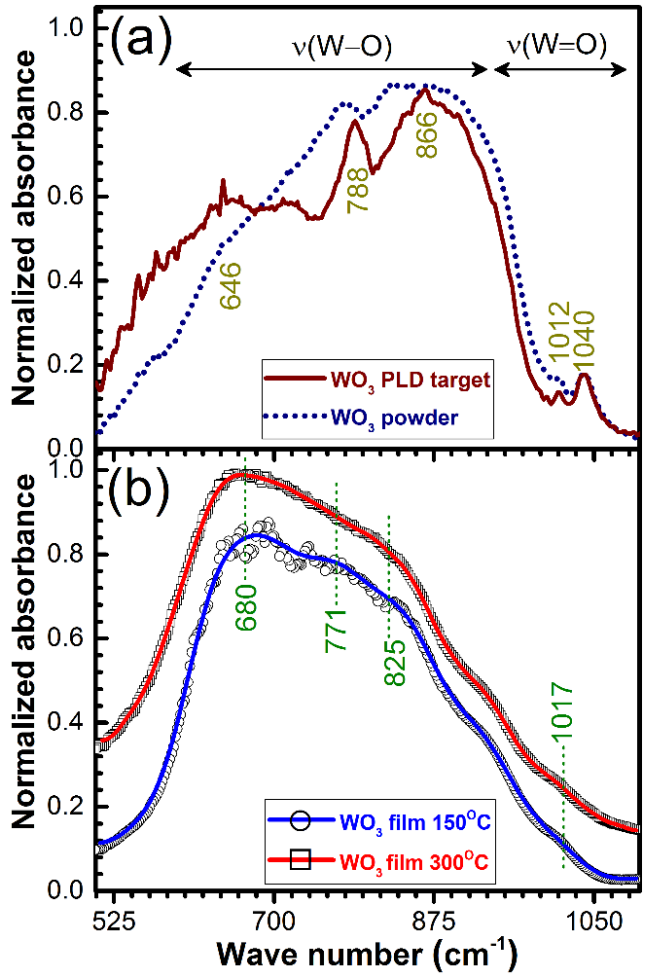
(a)
ν(W–O)
ν(W=O)
646
788
866
1012
1040
WO3 PLD target
WO3 powder
Normalized absorbance
(b)
680
771
825
1017
WO3 film 150°C
WO3 film 300°C
Normalized absorbance
Wave number (cm-1)
0.0
0.2
0.4
0.6
0.8
1.0
525
700
875
1050

Fig. 2.

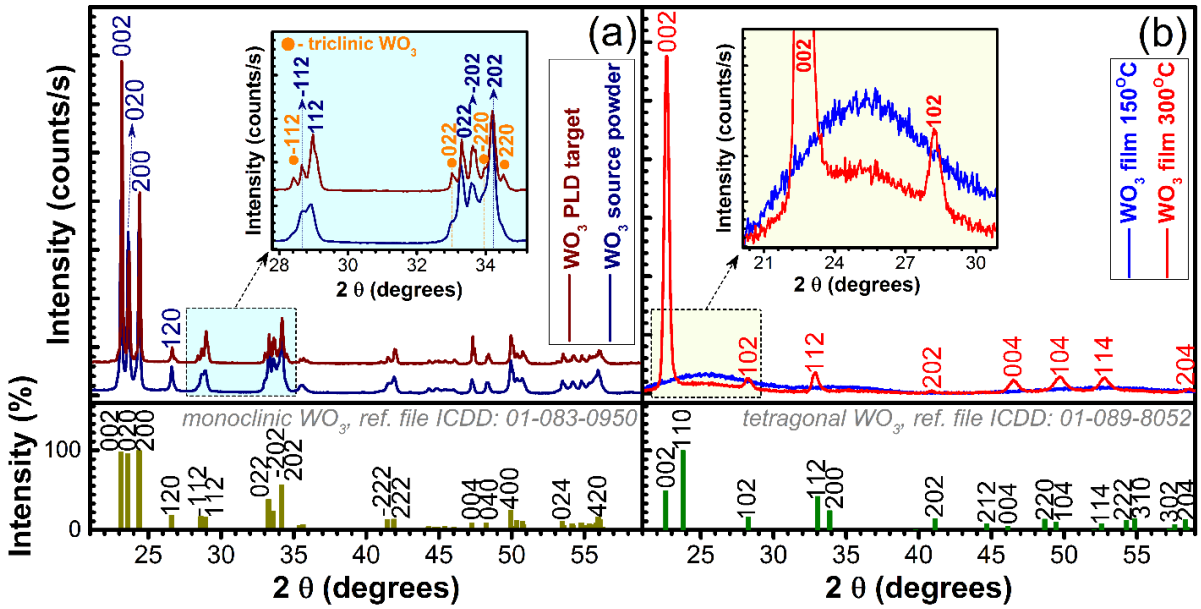
(a)
(b)
Intensity (counts/s)
Intensity (%)
2 θ (degrees)
- triclinic WO3
WO3 PLD target
WO3 source powder
WO3 film 150°C
WO3 film 300°C
monoclinic WO3, ref. file ICDD: 01-083-0950
tetragonal WO3, ref. file ICDD: 01-089-8052

Fig. 3.

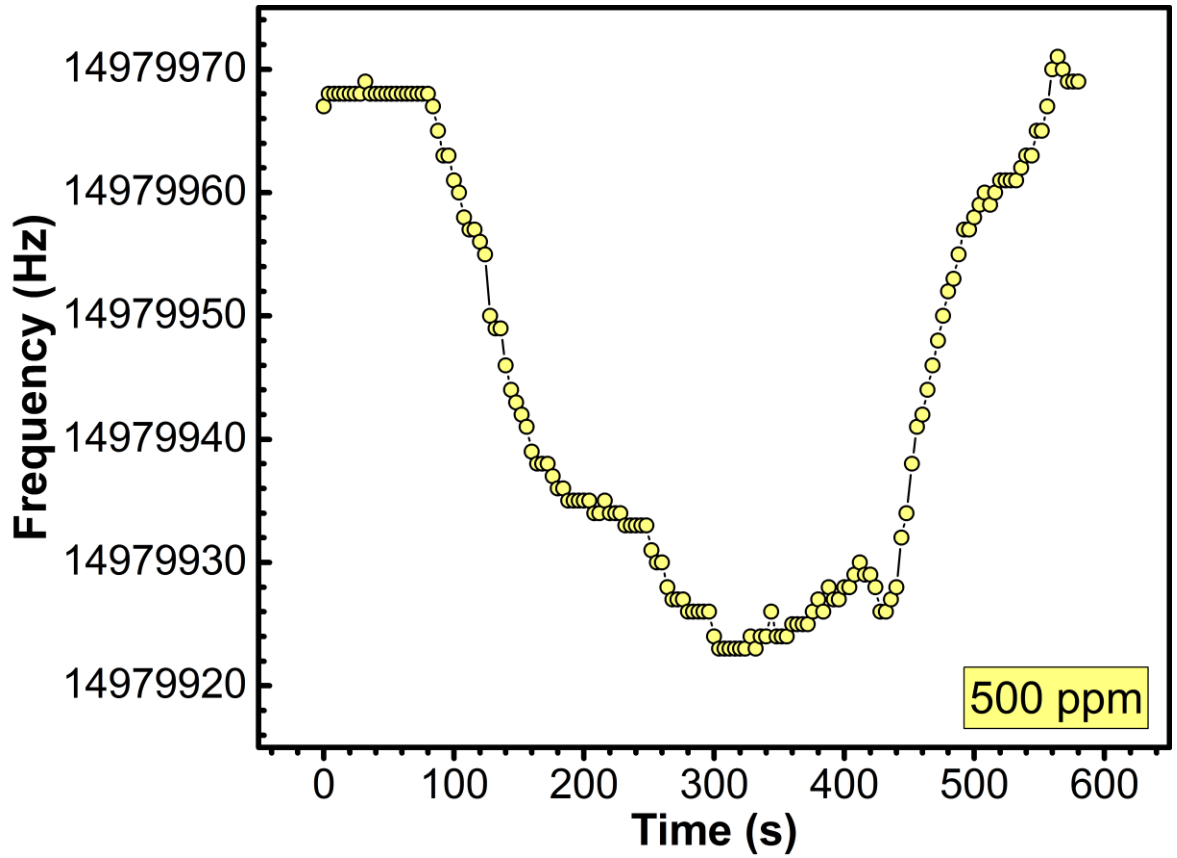
Frequency (Hz)
14979970
14979960
14979950
14979940
14979930
14979920
0
100
200
300
400
500
600
Time (s)
500 ppm

Fig. 4.

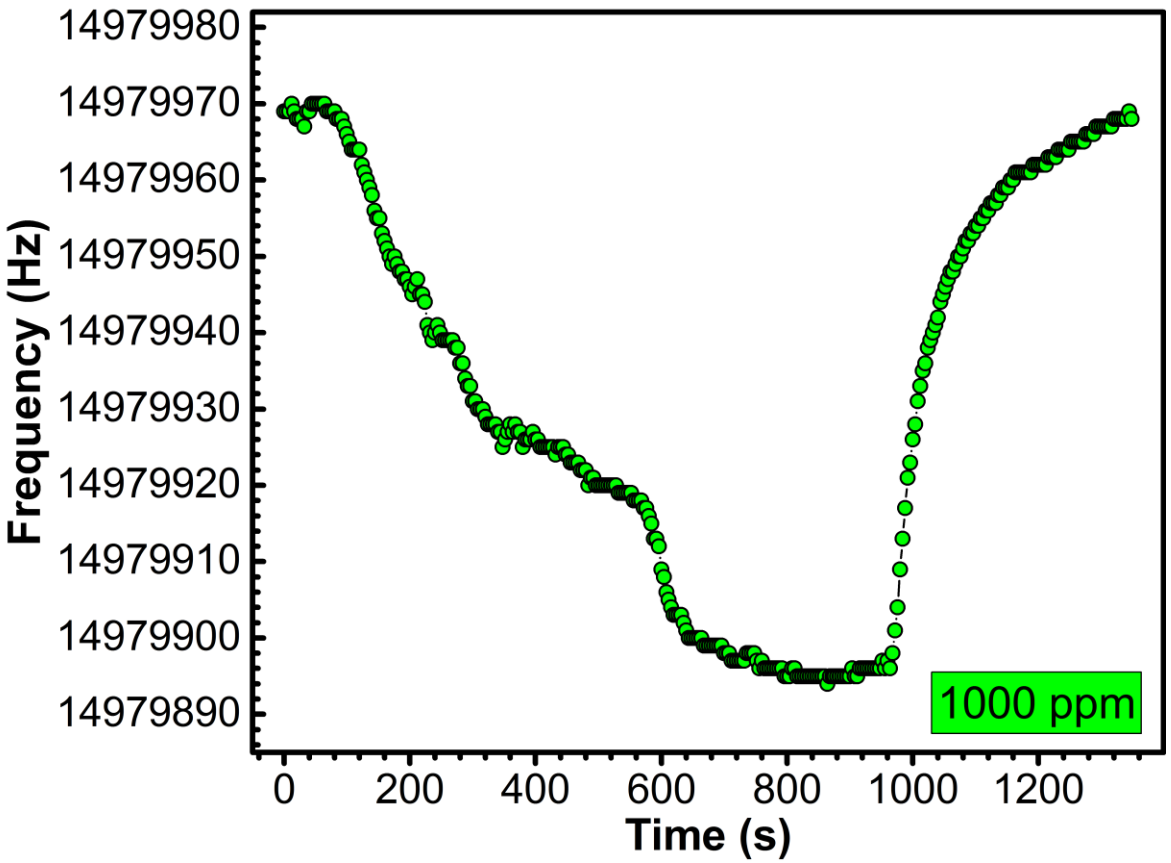
Frequency (Hz)
14979980
14979970
14979960
14979950
14979940
14979930
14979920
14979910
14979900
14979890
0
200
400
600
800
1000
1200
Time (s)
1000 ppm

Fig. 5